

## **Defects in Friction Stir Welding of Steel**

AL-MOUSSAWI, M and SMITH, Alan <<http://orcid.org/0000-0001-7868-8501>>

Available from Sheffield Hallam University Research Archive (SHURA) at:

<http://shura.shu.ac.uk/19110/>

---

This document is the author deposited version. You are advised to consult the publisher's version if you wish to cite from it.

### **Published version**

AL-MOUSSAWI, M and SMITH, Alan (2018). Defects in Friction Stir Welding of Steel. *Metallography, Microstructure, and Analysis*, 7, 194-202.

---

### **Copyright and re-use policy**

See <http://shura.shu.ac.uk/information.html>



# Defects in Friction Stir Welding of Steel

M. Al-Moussawi<sup>1,2</sup> · A. J. Smith<sup>1</sup>

Received: 14 December 2017 / Revised: 14 February 2018 / Accepted: 26 February 2018  
© The Author(s) 2018

## Abstract

Defects associated with friction stir welding of two steel grades including DH36 and EH46 were investigated. Different welding parameters including tool rotational and tool traverse (linear) speeds were applied to understand their effect on weld seam defects including microcracks and voids formation. SEM images and infinite focus microscopy were employed to identify the defects types. Two new defects associated with the friction stir welding process are introduced in this work. The first defect identified in this work is a microcrack found between the plunge and the steady state region and attributed to the traverse moving of the tool with unsuitable speed from the plunge-dwell to the steady state stage. The tool traverse speed has recommended to travel 20 mm more with accelerated velocity range of 0.1 from the maximum traverse speed until reaching the steady state. The maximum recommended traverse speed in the steady state was also suggested to be less than 400 mm/min in order to avoid the lack in material flow. The second type of defect observed in this work was microcracks inside the stirred zone caused by elemental precipitations of TiN. The precipitates of TiN were attributed to the high tool rotational speed which caused the peak temperature to exceed 1200 °C at the top of the stirred zone and based on previous work. The limit of tool rotational speed was recommended to be maintained in the range of 200-500 RPM based on the mechanical experiments on the FSW samples.

**Keywords** Friction stir welding · TiN precipitation · Microcracks · DH36 and EH46 steel grades · SEM

## Introduction

Despite many advantages associated with the friction stir welding (FSW) process, the technique does not always produce defect free joints [1]. Controlling the FSW process in order to produce high-quality weld joints is a challenge due to the number of parameters associated with the FSW process. Such parameters include independent (such as tool rotational/traverse speeds) and dependent (such as forces and torque) welding process parameters, tool material, tool design, workpiece material and thickness. The following types of defects were reported previously in FSW of aluminum and steel joints:

- *Wormholes, voids, and tunnels in the bottom of the weld joints* Probably due to insufficient heat input and the lack in material flow [1–3].
- *Kissing Bonds* Cracks but in close contact usually located at the weld root, they are materials in lack of chemical and mechanical bonding [4].
- *Root sticking* is caused by excessive heat and contact time resulting in the workpiece sticking to the backing plate [3].
- *Incomplete Fusion Laps* As a result of impurities present at the top surface and edges of the workpiece as there is no cleaning of these surfaces before FSW process [5].
- *Flash formation and material thinning*: caused mainly by excessive heat as a result of excessive axial forces [6].
- *Weld Root Flaw* Cracks starting from the bottom of the workpiece at uneven surfaces toward the welded zone [5].
- *Oxidation* Resulted from higher temperatures with no gas shield during the FSW process [7].

---

✉ M. Al-Moussawi  
b1045691@my.shu.ac.uk; inj.mun@atu.edu.iq

<sup>1</sup> Sheffield Hallam University, Sheffield, UK

<sup>2</sup> Al-Furat Al-Awsat Technical University, Kufa, Iraq

- *Lack-of-Fill Defect* Resulting mainly from losing material support at the trailing side of the tool due to excessive heat input [7].

A significant amount of data is reported in the literature on investigations into the types and sources of defects in FSW including numerical and experimental techniques. However, much of this has focused on low melting point alloys with far less information available about defect formation in FSW steels. Schmidt and Hattel [8] included the formation of the void in modeling the FSW by establishing the dwell and weld periods. The formation of the void at the lower advancing-trailing side of the probe/workpiece interface has interpreted as a lack of the contact between the tool and workpiece material because of the high traverse tool speed. Toumpis et al. [9] studied the formation of flaws during the FSW process of DH36 steel experimentally by examining the microstructure and carrying out fatigue test. They showed that the interruption in the surrounding phase led to a cavity caused by nonmetallic inclusions. Failla [10] related void defect formation to FSW tool travel speed. It was reported that increasing the linear travel speed reduced the heat input which resulted in a faster cooling of the material before this region becomes filled with stirred material. Tingey et al. [11] investigated defects in DH36 steel during FSW due to tool deviation from its centerline. It was found that ductile fracture was observed when the tool deviates by at least 2.5 mm and the critical tolerance to the tool centerline deviation should not exceed 4 mm. The material tensile strength was significantly reduced when the tool centerline deviation exceeds 4 mm. Stevenson et al. [5] studied the defects and its effects on materials properties including fatigue and microstructure evolution of FSW 6-mm-thickness DH36 steel. Defects were divided into several types including incomplete fusion paths arising from impurities on the top surface of the workpiece as there is no preparation of plate edges prior the FSW process. Additionally, weld root flaws at the plate bottom interpreted as a result of insufficient tool plunge depth and deviation of the tool from the normal centerline. Lower embedded flaws (Type 1) as a result of the lack in material stirring due to lower heat input were reported. Lower embedded flaws (Type 2) which exist in the SZ of the welded joints was the result of the lack in axial force. Upper embedded flaw (swirl zone) at the AS was reported as a result of combination of two flows coming from shoulder and probe. Connectivity flaws between TMAZ and HAZ boundary has also been found in the welded joints. It was found that fatigue resistance decreased significantly with the existence of flaws at the weld root, especially wormholes defects. The longitudinal residual stresses measured by the hole drilling technique were also found to reduce the fatigue resistance [5]. As the

embedded flaws have sharp edges, they can act as stress concentration points leading to a crack initiation toward the top and bottom surfaces of the workpiece [5]. Toumpis et al. [12] stated that flaws in FSW of DH36 steel can be created when the heat input from the tool is insufficient, and thus, a lack in material flow may occur. The authors also found in another experiment including hot compression test with wide ranges of temperatures and strain rates that the flow stress increases with the decrease in temperature and the increase in strain rate. This was the case when tool traverse speed increases, leading to a lack in material flow and defects formation [5]. Morisada et al. [13] showed experimentally, by the aid of an x-ray transmission real-time imaging system and by monitoring the three-dimensional material flow during FSW of steel, that defects formation on the advancing side is the result of material stagnation. Gibson et al. [14] showed that flaws in FSW are the result of unsuitable welding parameters and the source of surface breaking flaws comes from surface oxides penetration into the stirred zone.

Workpiece geometry can also be a challenge especially in material with high thickness, Seaman and Thompson [7] investigated challenges in FSW of thick steel and found that the possibility of defects formation in the welded joints increases with increasing workpiece thickness due to the increase in thermal diffusion distance. As the time to diffuse heat by the tool into the depth of workpiece is insufficient to create a uniform distribution of temperature throughout the thickness of the weld, isotherms will develop inside the FSW region. In this case, the top of the workpiece around the tool shoulder is expected to experience better stirring conditions than the bottom of the weld; thus, the possibility of defects formation such as wormholes will increase. The authors attributed defects to a lack of forging forces or the heat imbalance. Defects such as lack-of-fill were also found in the thick steel joints when the tool rotational speed and axial force increased, causing a loss in material support behind the tool. Reducing heat input by increasing weld heat extraction or by increasing the shoulder radius has been suggested in order to constrain the stirred material.

The effect of dependent welding parameters such as welding forces on defect formation has also been investigated. Kim et al. [6] studied the effects of plunge forces on FSW of aluminum die casting and found that increasing plunge downforce results in improved weld quality. They found that excessive heat input can increase the possibility of flash forming, while insufficient heat input or abnormal stirring may cause a cavity defect.

Previous studies reported in the literature did not investigate the possible effect of elemental precipitation/segregation on defects formation. Additionally, there is no previous investigation of the effect of tool traverse speed

especially when traveling from the plunge to steady state region. In this work, the defects in FSW of two types of steels including DH36 and EH46 grades have been investigated. SEM images and IFM mechanism were employed to reveal these defects in the stirred zone. Mechanical tests including tensile and fatigue were applied to investigate the effect of defects on the physical properties. Recommendations have been established in order to avoid defects and to improve the welded joints.

## Materials and Methods

Two FSW samples of 6–8 mm-thick hot rolled DH36 and two samples of 14-mm-thick EH46 steel grades were investigated; chemical composition as supplied by the manufacturer is shown in Tables 1 and 2. Friction stir welding has been carried out at TWI/Yorkshire by using PowerStir FSW machine; hybrid FSW PCBN tool (commercially known as Q70) with shoulder diameter of 24- and 5.7-mm probe length was used for welding 6- and 8-mm-thick plates. Another PCBN tool with diameter of 38- and 11-mm probe length was used for welding 14-mm-thick plates. Note that maximum plunge depth expected from this tool is 12 mm. The welding parameters including tool rotational/traverse speeds, plunge depth, torque, and forces are shown in Table 3.

## SEM and EDS

The weld defects were investigated by accurately cutting the sample from the longitudinal direction between the advancing and retreating sides using miter saw with 1-mm cutting wheel. Defects inside the SZ microstructure were revealed by SEM technique after grinding, polishing and etching by 2% Nital solution. EDS-based SEM was used to detect the type of elemental precipitations. The SEM produced high-quality and high-resolution images of microconstituents by employing the secondary electron (SE) imaging mode with an accelerated voltages (10–20 kV) which gives relatively high penetration. The working distance (WD) used was 5 mm but in some cases altered (decreased or increased) to enhance the contrast at high magnification.

## Fatigue and Tensile Tests

Samples for tensile and fatigue test (dimension shown in Fig. 1) were cut from the steady state welding by using

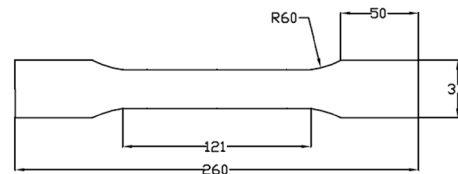


**Fig. 1** Tensile and fatigue sample dimensions (in mm) according to EN-BS 895:1995 and BS 7270 standards [5]

**Table 1** Chemical composition (wt.%) of DH36 as received from the manufacturer

C	Si	Mn	P	S	Al	N	Nb	V	Ti	Cu	Cr	Ni	Mo
0.16	0.15	1.2	0.01	0.005	0.043	0.02	0.02	0.002	0.001	0.029	0.015	0.014	0.002

**Table 2** Chemical composition (wt.%) of EH46 steel grade

C	Si	Mn	P	S	Al	N	Nb	V	Ti
0.20	0.55	1.7	0.03	0.03	0.015	0.02	0.03	0.1	0.02

**Table 3** Welding conditions of FSW DH36 and EH46 steel at the steady state

Weld no.	Tool rotational speed RPM	Traverse speed, mm/min	Rotational/traverse speeds, rev/mm	Plunge depth, mm	Average spindle torque, N.m	Average tool torque, N.m	Axial force (average), KN	longitudinal force (average), KN	Heat input $\frac{\omega \times \text{torque}}{v}$ , W/mm
W <sub>1D</sub>	200	100	2	5.8	278	105	57.55	12.8	210
W <sub>2D</sub>	550	400	1.375	5.8	163	62	47	12	64.625
W <sub>1E</sub>	150	50	3	11.67	300	114	66	13	342
W <sub>2E</sub>	150	100	1.5	11.67	450	171	72	14	256.5

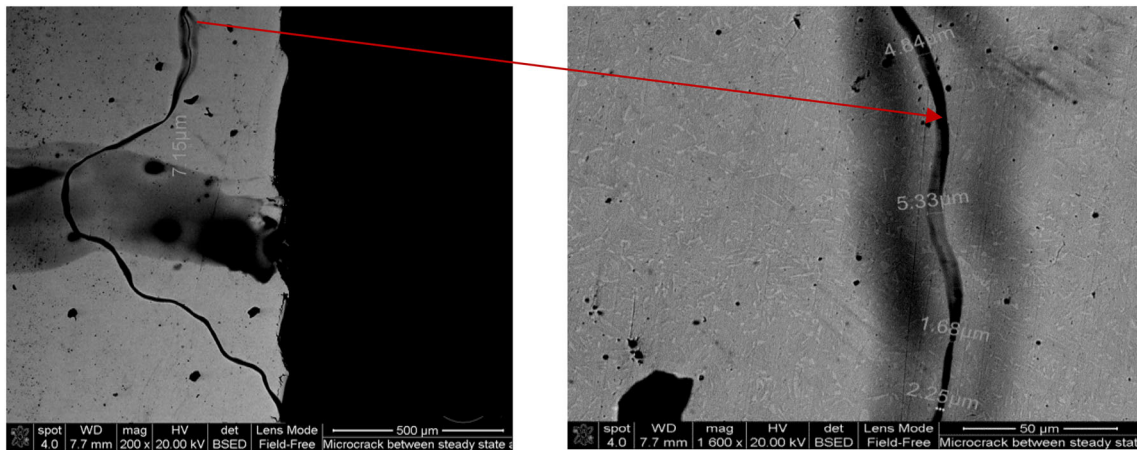


**Fig. 2** Microcrack started from the top surface of FSW DH36  $W_{1D}$  between steady state and the plunge regions. (a) low magnification, (b) high magnification. The sample was cut in the direction of the weld line

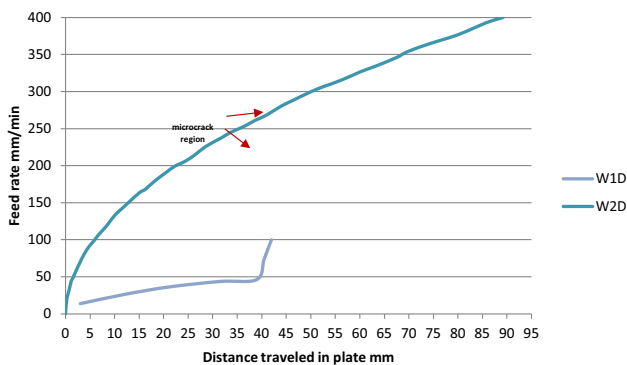


**Fig. 3** Feed rate and the distance travelled by tool in the DH36 plates just before the steady state

water jet technique in order to reduce distortion associated with cutting by a heat source, the cut was in a direction normal to the welding line. Samples taken from plate were prepared for the Fatigue test based on BS 7270 standard. The sides of samples were polished in the longitudinal direction to reduce the effects of any sharp edges that act as a stress concentration. The tensile samples were tested using a machine equipped with a 250-KN load cell, preload was 2 MPa, and test speed was 0.0067 1/s. Fatigue tests were carried out according to BS 7270 standard with load set of 0.8 of the yield stress, amplitude of 137.5 MPa and stress frequency of 10 HZ during the testing program [5].

### Infinite Focus Microscopy (IFM)

Infinite focus microscopy IFM has been employed to create accurate optical light microscopy images of the welded joint. The IFM is a device based on optical 3-dimensional measurements which has the ability to varying the focus in order to obtain a 3D vertical scanned image of the surface.

The scanned area of interest can be transferred into a 3D image by the aid of Lyceum software; thus, the surface area can be calculated accurately.

### Results

Defects in the as-received FSW samples were investigated by the aid of IFM and SEM-EDS. Two defects were identified using the specific conditions during the FSW process and are introduced in this work. The first type of defect is a microcrack in the longitudinal direction between plunge and steady state region. The second types of defects are microcracks caused by interstitial elements precipitation/segregation. The first type of defects was found in FSW DH36  $W_{1D}$  (8-mm-thick plate) as shown in Fig. 2a and b. The feed rate of  $W_{1D}$  has been compared to  $W_{2D}$  as shown in Fig. 3. Possible defects of high tool speeds of DH36 ( $W_{2D}$ ) in the longitudinal direction between plunge/steady state and also in the steady state are shown in Fig. 4a and b, respectively. Defects of high tool speeds (DH36  $W_{2D}$ ) detected by IFM shown in Fig. 5 were also investigated by SEM as shown in Fig. 6a and b. Non-metallic layer has been found in the higher tool speeds joints (DH36  $W_{2D}$ ) located between the SZ and HAZ as shown in Fig. 7a and b.

A void found in FSW of 14-mm-thick EH46 steel  $W_{2E}$  at steady state 9 mm from the top of the plate surface at the advancing side (AS) as measured by the IFM technique is shown in Fig. 8 and in the SEM images of Fig. 9a and b.

Defects in the form of microcracks due to elemental precipitation/segregation in both DH36 and EH46 are shown in Figs. 10-12.

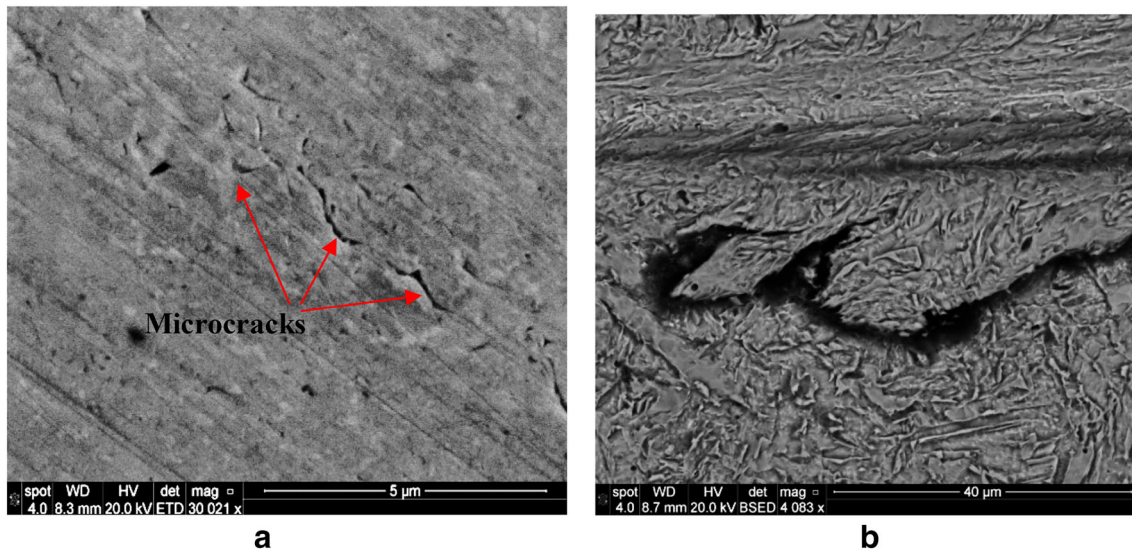


**Fig. 4** Microcracks inside the SZ. (a) Between plunge-steady state regions of FSW DH36  $W_{2D}$  (b) between plunge-steady state regions of FSW DH36  $W_{2D}$ . The sample was cut in the direction of the welding line

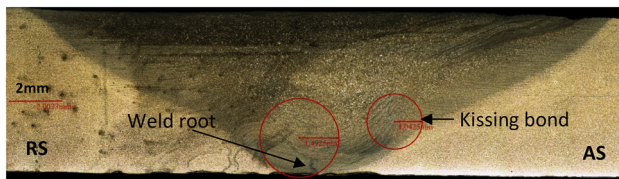


**Fig. 5** Weld root and kissing bond in 6-mm FSW DH36 ( $W_{2D}$ )

## Discussion

$W_{1D}$  FSW DH36 has showed a microcrack of 2–5  $\mu\text{m}$  width as shown in Fig. 2a and b when the tool has travelled a distance 38–42 mm in the plate weld line just before the steady state. Figure 3 compares curves of feed rate with the distance travelled by the FSW tool just before the start of the steady state of  $W_{1D}$  with  $W_{2D}$ . The figure shows that  $W_{1D}$  experienced rapid traverse speed (from 50 to 100 mm/min with distance travelled of 2 mm), whereas in  $W_{2D}$  the travelled distance was 5 mm with a gradual increase (50 mm/min) in traverse speed. Insufficient heat coming from low tool rotational speed and the sudden increase in traverse speed have been caused a lack in material flow of  $W_{1D}$  which in turn has resulted in the mentioned crack initiation. The crack is initiated from the top surface of the weld toward the steady state of the SZ depth. This type of defects can weaken the weld joints, and thus, poor mechanical properties are expected.  $W_{2D}$  FSW DH36 has showed different types of microcracks created inside the SZ in the direction of welding line between plunge-steady state region as shown in Fig. 4a and b, respectively. Despite the higher rotational speed of the tool (500 RPM) compared to  $W_{1D}$ , the higher traverse speed (400 mm/min)

overrides the rotational speed. The lack in material flow due to low heat input can be the main reason for these defects as reported in previous work [3, 5, 15].

Figure 5 shows  $W_{2D}$  macrograph scanned by IFM technique; two types of defects have been detected including weld root defect at the weld joint bottom and kissing bond defect at the AS of the weld. The first macrocrack (weld root defect) which starts from plate back and reach 2 mm length into the SZ as shown in Fig. 6a can be attributed to the lack in material flow as a result of high traverse speed. This type of defect coincides with previous study by Stevenson et al. [5] which specified as weld root defects resulted from the lack in plunge depth of the FSW tool. The insufficient heat input accompanied by the lack in material flow may be caused in a stagnant zone formation as proved by modeling studies [15]. The material in this region will be vulnerable to crack formation under the normal plunge force, so any uneven surface or sharp edge will act as a stress concentration point as labeled in Fig. 6a. The second crack on the AS of  $W_{2D}$  at the weld root as shown in Fig. 6b can be classified as a kissing bond which is materials in lack of chemical and mechanical bonding but in close contact. This type of defect is difficult to identify by using the nondestructive tests such as ultrasound, and thus, it needs to be investigated carefully using optical or SEM scanning of a polished etched sample. The size of kissing bond defect can affect on the mechanical properties of the weld joints especially fatigue strength [4].

Figure 7a and b shows a nonmetallic layer of (Fe, Mn, Si, Al and O) as identified by SEM–EDS between the SZ and HAZ. This was found in  $W_{2D}$  at (a) plunge period with 10  $\mu\text{m}$  width and (b) at steady state period with width of 1.3  $\mu\text{m}$ . This type of defects can be the result of higher tool

**Fig. 6** SEM of the first and second defects of DH36 6-mm  $W_{2D}$  shown in Fig. 5. (a) Weld root, (b) kissing bond

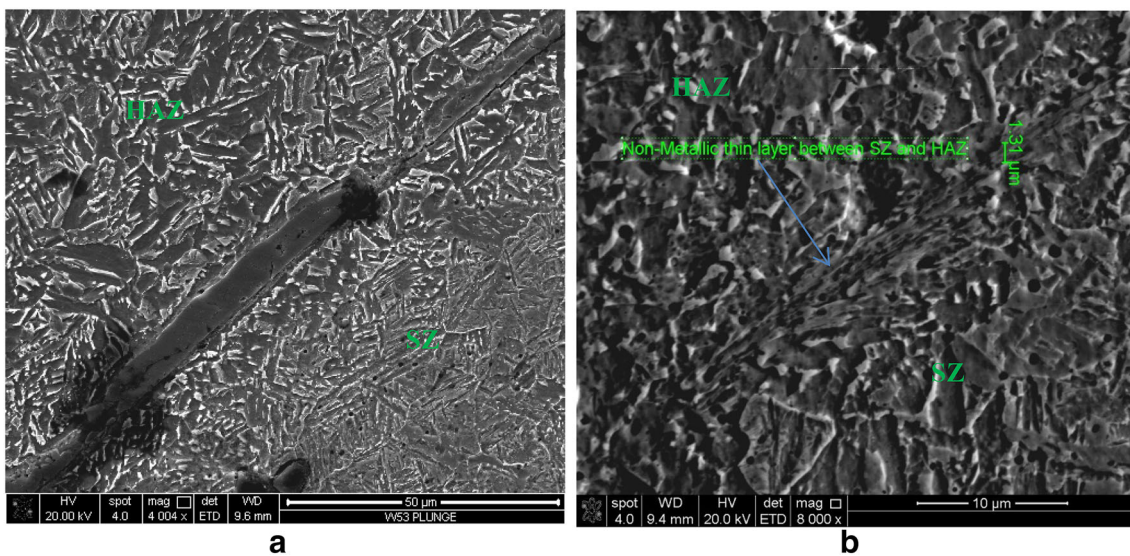
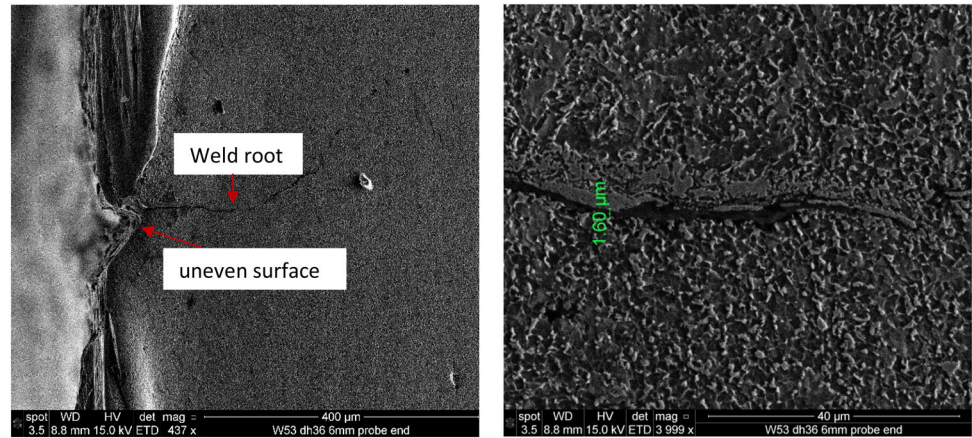


**Fig. 7** Nonmetallic layer of (Fe, Mn, Si, Al and O) between the SZ and HAZ found in  $W_{2D}$ , (a) 10  $\mu\text{m}$  at plunge period, (b) 1.3  $\mu\text{m}$  at steady state period

rotational speed which caused in a temperature close to the local melting, and thus, elemental segregation of Mn, Si, Al and O has occurred [16]. The experiments on the same grade of steel showed that elemental precipitation/segregation only occurs when the temperature equals or exceeds 1450  $^{\circ}\text{C}$  [16]. The tool centrifugal forces caused influx of these elements toward the edge of the SZ, and thus, they have deposited in the region between the SZ and HAZ.

Void on the AS of FSW EH46  $W_{2E}$  as shown in Fig. 8 has been found at 9.8 mm distance from the top surface of the weld joint between the SZ and HAZ as detected by the IFM. Figure 9a shows SEM image of the void which has a diameter of about 250  $\mu\text{m}$ ; high amount of BN particles which separated from the PCBN FSW tool were also found near and around the void as shown in Fig. 9b. The void defect is likely to happen as a result of the lack in material stirring due to the high tool traverse speed. This result

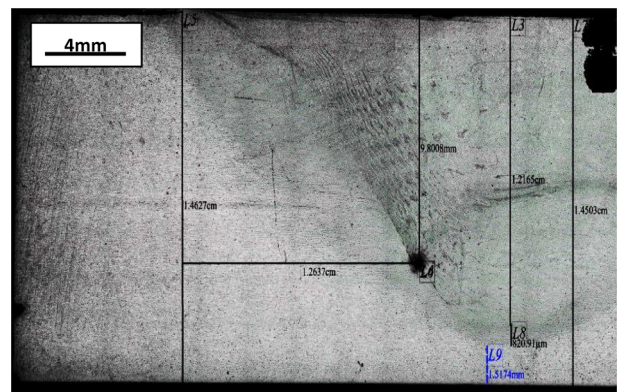


**Fig. 8** A void found in EH46 steel  $W_{2E}$  (steady state) in AS

coincides with previous work on FSW process where Schmidt and Hattel [17] included the formation of the void

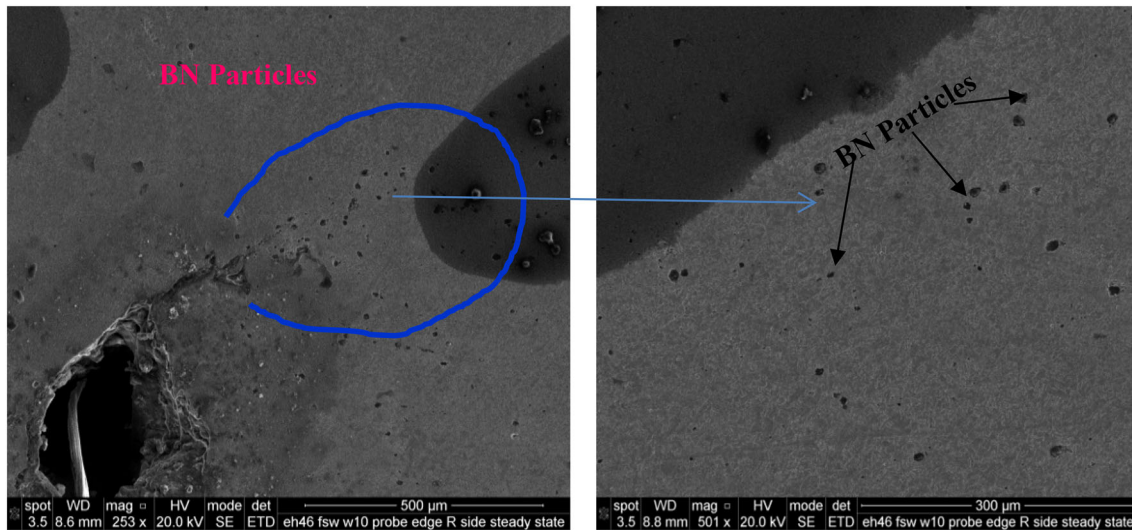


**Fig. 9** High amount of BN particles found near the void at AS, EH46 steel  $W_{2E}$  (steady state)

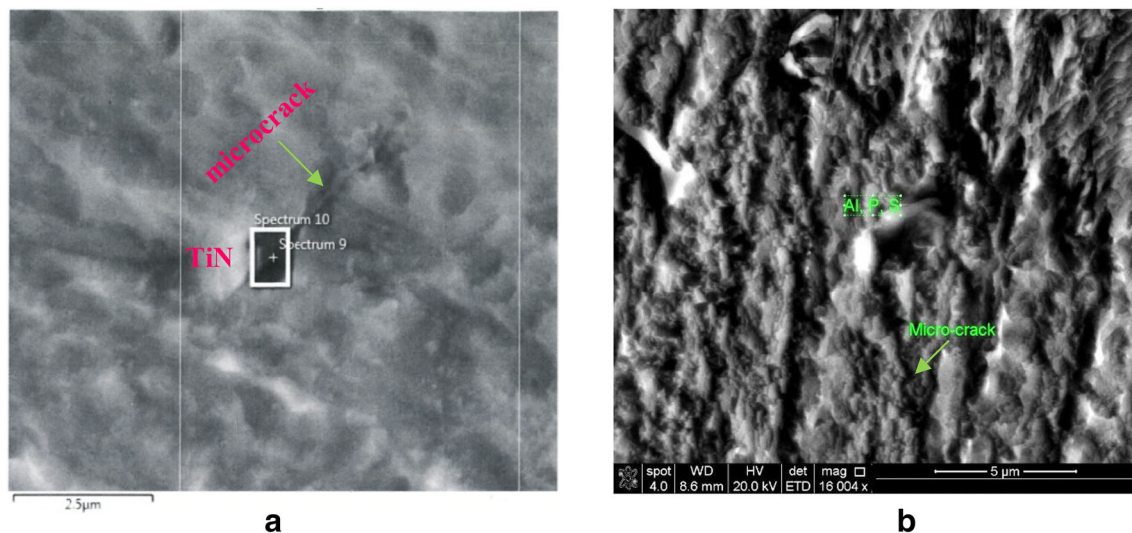


**Fig. 10** SEM of the SZ of DH36  $W_{2D}$  (a) microcrack caused by TiN particle, (b) microcrack caused by Al P S elemental precipitates

in modeling the FSW by establishing the dwell and steady state periods and interpreted its formation at the lower advancing-trailing side of the probe/workpiece interface as a lack in contact between the tool and matrix interface which in turn coming from the high traverse tool speed. Toumpis et al. [9] also explained the formation of voids experimentally; it was shown that the interruption in the surrounding phase has led to a minor cavity caused by nonmetallic inclusions. Failla [10] related the void defect formation to the FSW tool travel speed. It was found that the increase in linear travel speed has caused in a fast cooling to the material before the region becomes filled with the stirred material, leading to the void formation.

Figure 10a and b shows SEM images which include TiN and Al, P, S precipitates, respectively, in the SZ

microstructure of FSW DH36  $W_{2D}$  as identified by SEM-EDS. This weld also contained microcracks initiated from TiN particle and also Al, P, S. This elemental precipitation especially TiN in the SZ microstructure is usually the result of a high peak temperature experience exceeds 1200 °C [18–20]. Orlando et al. [21] proved by the aid of optical microscope and SEM that cubic TiN particles can cause voids during the tensile test of IF steels. They interpreted this type of defect as a fragmentation of weak particles coming from stresses generated from TiN particles corners. An extensive study about microphysical process of cleavage fracture in steel can be found in Chen and Cao [22] which focuses on the steps of crack initiation, nucleation and propagation under internal residual stresses caused by TiN precipitation. Figure 11a and b shows microcracks

caused by TiN particles (exceeds 1  $\mu\text{m}$ ) in FSW EH46  $W_{2E}$  SZ at steady state and DH36 sample heat-treated to 1300  $^{\circ}\text{C}$  with slow cooling rate (cooling inside furnace), respectively. Figure 12 shows elemental segregation of Mn, Si, Al and O in the SZ of FSW DH36  $W_{2D}$  which can also play as a stress concentration and microcracks initiation sites.

Mechanical properties of FSW joints are expected to decrease with the existence of the previously mentioned defects. Samples of tensile test including FSW DH36  $W_{2D}$  have been failed outside the welded region which means that welding is still accepted despite the presence of microcracks coming from elemental precipitations. The tensile strength is also increased to 580 MPa for  $W_{1D}$  compared to the strength of parent metal (475 MPa) as a

result of microstructure refinement. Samples of fatigue test of  $W_{2D}$  have been showed a decrease in fatigue resistance compared to  $W_{1D}$  as a result of defects existence in the SZ of the welded joints. The average cycles of failure for  $W_{2D}$  were 115,078 cycles, whereas  $W_{1D}$  has showed more resistance to fatigue failure with failure cycles reached to 642,935. Comparing the FSW process with SAW, the fatigue resistance has improved significantly as a result of microstructure refinement [9]. Microcracks coming from unsuitable welding parameters and also from the elemental precipitation, especially TiN, have certainly played the main role in this reduction in fatigue resistance. It is recommended to reduce the peak temperature when welding this type of steel by reducing the tool rotational speed below 500 RPM in order to avoid elemental precipitation/segregation.

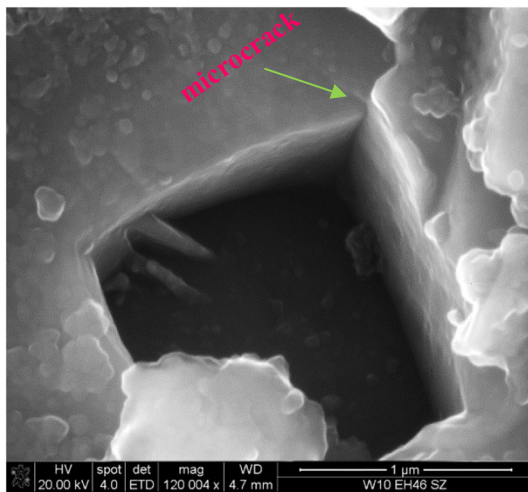


**Fig. 11** SEM images show microcracks caused by TiN precipitates (exceeds 1  $\mu\text{m}$ ), FSW EH46  $W_{2E}$  SZ at steady state

## Conclusion

In conclusion, defects associated with the FSW process of DH36 and EH46 steel grades have been studied. High tool traverse speed as in DH36  $W_{2D}$  and in EH46  $W_{2E}$  was found to cause defects formation such as voids, weld root defect and kissing bonds. The lack in material flow as a result of stagnant zone formation was the main reason of these defects. Microcracks between the plunge and steady states are also examples of defects caused by the lack in material flow resulted from using unsuitable tool traverse speed. Defects were also found in the FSW joints microstructure as a result of the increase in welding temperature higher than 1250  $^{\circ}\text{C}$  when using high tool rotational speed exceeds 500 RPM. Mainly elemental precipitation such as TiN and elemental segregation of Mn,

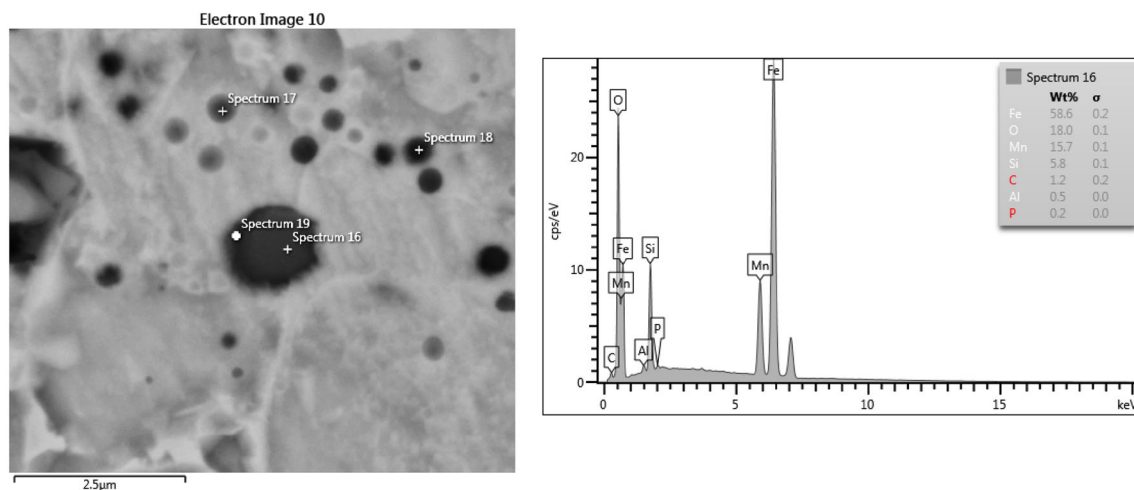


**Fig. 12** SEM-EDS shows elemental segregation of Mn, O and Si in the SZ of FSW DH36 at high tool speeds ( $W_{2D}$ )

Si, Al and O was the results of using high tool rotational speed. These elementals precipitation/segregation can cause in microcracks and stress concentration initiation sites causing in decreasing the mechanical properties of the welded joints.

**Acknowledgments** The author would like to thank the ministry of higher education/Iraq for funding this work. The authors also would like to thank TWI company for providing data and samples.

**Open Access** This article is distributed under the terms of the Creative Commons Attribution 4.0 International License (<http://creativecommons.org/licenses/by/4.0/>), which permits unrestricted use, distribution, and reproduction in any medium, provided you give appropriate credit to the original author(s) and the source, provide a link to the Creative Commons license, and indicate if changes were made.

## References

1. A. Pradeep, A review on friction stir welding of steel. *Int. J. Eng. Res. Dev.* **3**(11), 75–91 (2012). e-ISSN: 2278-067X, p-ISSN: 2278-800X. [www.ijerd.com](http://www.ijerd.com)
2. K. Elangovan, V. Balasubramanian, Influences of pin profile and rotational speed of the tool on the formation of friction stir processing zone in AA2219 aluminium alloy. *Mater. Sci. Eng. A* **459**(2007), 7–18 (2007)
3. A.K. Lakshminarayanan, V. Balasubramanian, Understanding the parameters controlling friction stir welding of AISI 409 M ferritic stainless steel. *Met. Mater. Int.* **17**(6), 969–998 (2011)
4. R. Ruzek, M. Kadlec, Friction stir welded structures: kissing bond defects. *Int. J. Terraspace Sci. Eng.* **6**(2), 77–83 (2014)
5. S. Ryan, A. Toumpis, A. Galloway, Defect tolerance of friction stir welds in DH36 steel. *Mater. Des.* **87**(15), 701–711 (2015)
6. Y.G. Kim, H. Fujii, T. Tsumura, T. Komazaki, K. Nakata, Three defect types in friction stir welding of aluminum die casting alloy. *Mater. Sci. Eng. A* **415**, 250–254 (2006)
7. J.M. Seaman, B. Thompson, Challenges of friction stir welding of thick-section steel, in *Proceedings of the Twenty-First International Offshore and Polar Engineering Conference*, Maui, Hawaii, USA, 2011, 19–24 June 2011
8. S. Cater, Forge welding turns full circle: friction stir welding of steel. *Ironmak. Steelmak.* **40**(7), 490–495 (2013). <https://doi.org/10.1179/0301923313Z.000000000224>
9. A. Toumpis, A. Gallawi, H. Polezhayeva, L. Molter, Fatigue assessment of friction stir welded DH36 steel. *Frict. Stir Weld. Process.* **VIII**, 11–19 (2015)
10. D.M. Failla, Friction stir welding and microstructure simulation of HSLA-65 and austenitic stainless steels, Thesis, The Ohio State University, 2009
11. C. Tingey, A. Galloway, A. Toumpis, S. Cater, Effect of tool centreline deviation on the mechanical properties of friction stir welded DH36 steel. *Mater. Des.* (1980–2015) **65**, 896–906 (2015)
12. A. Toumpis, A. Gallawi, S. Cater, N. McPherson, Development of a process envelope for friction stir welding of DH36 steel—a step change. *Mater. Des.* **62**, 64–75 (2014)
13. Y. Morisada, T. Imaizumi, H. Fujii, Clarification of material flow and defect formation during friction stir welding. *Sci. Technol. Weld. Join.* **20**(2), 130–137 (2015)
14. B.T. Gibson, D.H. Lammlein, T.J. Prater, W.R. Longhurst, C.D. Cox, M.C. Ballun, Friction stir welding: process, automation, and control. *J. Manuf. Process.* **16**, 56–73 (2014)
15. M. Al-Moussawi, A.J. Smith, A. Young, S. Cater, M. Faraji, Modelling of friction stir welding of DH36 steel. *Int. J. Adv. Manuf. Technol.* (2017). <https://doi.org/10.1007/s00170-017-0147-y>
16. M. Almoussawi, A.J. Smith, M. Faraji, S. Cater, Segregation of Mn, Si, Al, and oxygen during the friction stir welding of DH36 steel. *Metallogr. Microstruct. Anal.* **6**, 569 (2017). <https://doi.org/10.1007/s13632-017-0401-6>
17. R.M. Hooper, J.I. Shakib, C.A. Brookes, Microstructure and wear of TiC cubic BN tools. *Mater. Sci. Eng. A* **A106**, 429–433 (1988)
18. W. Ming-lin, G. Cheng, S. Qiu, P. Zhao, Y. Gan, Roles of titanium-rich precipitates as inoculants during solidification in low carbon steel. *Int. J. Miner. Metall. Mater.* **17**(3), 276–281 (2010)
19. S. Yamini, Effect of titanium additions to low carbon, low manganese steel on sulphide precipitation, Ph.D. theses, University of Wollongong, 2008
20. Y. Zhang, G. Xu, M.X. Zhou, H.L. Yang, M. Wang, The effect of reheating temperature on precipitation of a high strength microalloyed steel. *Appl. Mech. Mater.* **508**, 8–11 (2014)
21. O. León-García, R. Petrov, L.A.I. Kestens, Void initiation at TiN precipitates in IF steels during tensile deformation. *Mater. Sci. Eng. A* **527**, 4202–4209 (2010)
22. J.H. Chen, R. Cao, *Micromechanism of Cleavage Fracture of Metals, Chapter 3, Copyright* © 2015 (Elsevier Inc, Amsterdam, 2015), pp. 81–140